

# VMem: Consistent Interactive Video Scene Generation with Surfel-Indexed View Memory

Runjia Li Philip Torr Andrea Vedaldi Tomas Jakob  
University of Oxford

{runjia, phst, vedaldi, tomj}@robots.ox.ac.uk

[v-mem.github.io](https://v-mem.github.io)

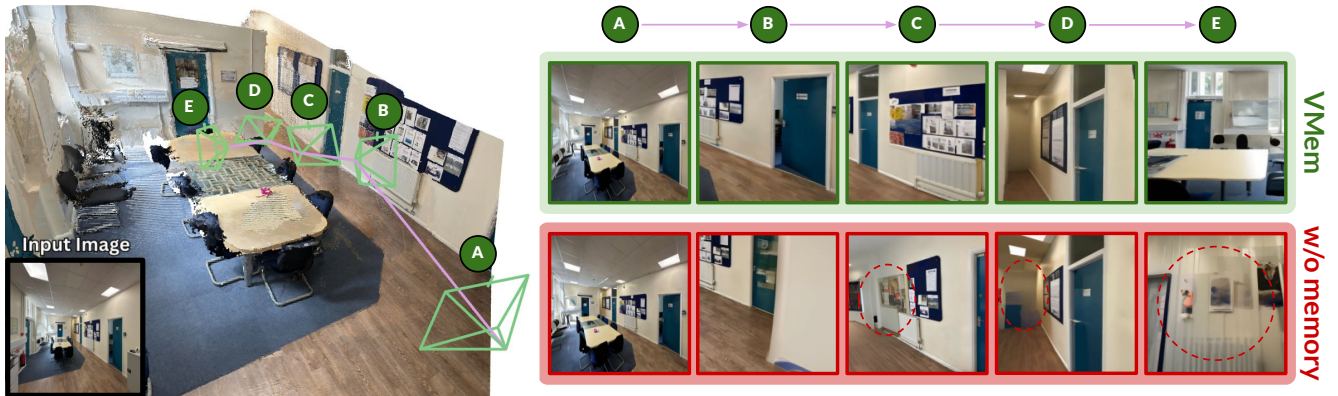


Figure 1. VMem enables interactive scene generation from a single image along user-specified trajectories in an auto-regressive manner. The **green** region shows results with memory, maintaining consistency when generating previously observed parts of the scene. The **red** region, without memory, exhibits visual drift highlighted with red ellipses, demonstrating the effectiveness of VMem for consistent scene generation.

## Abstract

We propose a novel memory mechanism to build video generators that can explore environments interactively. Similar results have previously been achieved by out-painting 2D views of the scene while incrementally reconstructing its 3D geometry, which quickly accumulates errors, or by video generators with a short context window, which struggle to maintain scene coherence over the long term. To address these limitations, we introduce Surfel-Indexed View Memory (VMem), a mechanism that remembers past views by indexing them geometrically based on the 3D surface elements (surfels) they have observed. VMem enables the efficient retrieval of the most relevant past views when generating new ones. By focusing only on these relevant views, our method produces consistent explorations of imagined environments at a fraction of the computational cost of using all past views as context. We evaluate our approach on challenging long-term scene synthesis benchmarks and demonstrate superior performance compared to existing methods in maintaining scene coherence and camera control.

## 1. Introduction

We consider the problem of generating long videos that explore an imagined space following a camera path specified interactively by the user. In this paradigm, the user tells the model which camera path to follow for the next few frames, observes the generated content, and then decides where to explore next based on what they have seen. For example, a possible exploration of a house may involve visiting the kitchen, the living room, and the bathroom, eventually returning to the kitchen. Throughout the video, the scene must remain consistent, ensuring that the kitchen looks the same upon return. The ability to generate such videos is essential for immersive applications such as games, where players can navigate generated worlds. However, even recent large-scale interactive video generators such as Google’s Genie 2 [21] struggle to achieve this goal.

This problem has so far been addressed by two types of methods. First, *out-painting-based* methods [7, 12, 16, 17, 19, 22, 25, 27, 37, 42] iterate between generating new 2D views of the scene and estimating its 3D geometry. They use the estimated geometry to partially render a new viewpoint and then employ an out-painting model to complete the missing parts, thus adding one more image to the col-

lection. However, errors in out-painting, 3D reconstruction, and stitching accumulate over time, leading to severe degradation of the generated content after a short while.

Second, *multi-view/video-based* methods [21, 23, 26, 36, 41] condition the generation of a novel view on previously generated views using a geometry-free approach that does not explicitly estimate the scene geometry. While this avoids the accumulation of errors in the reconstructed 3D scene geometry, it comes at a high computational cost, limiting the number of conditioning views to a small context window consisting of only the most recent few frames. This constraint negatively impacts the long-term consistency of the generated images.

In this work, we revisit the second class of methods and propose conditioning not on the most recently generated views, but on the *most relevant ones* for generating the next image, thereby maintaining a high degree of consistency within a limited computational budget. Given a novel viewpoint of the scene, the most relevant past views are those that have already observed the parts of the scene currently being generated. This implies that, for each part of the scene, we must remember which views have previously observed it and allow one to retrieve them from memory.

To achieve this, we introduce the *Surfel-Indexed View Memory*, abbreviated as *VMem*, a memory mechanism that anchors previous views to the 3D surface elements they observe. Given a new viewpoint, we retrieve the past views that best capture the currently observed surfaces and use them to condition the generation of the novel view. To create the memory, we estimate the geometry of each new view using an off-the-shelf point map predictor. This is similar to out-painting methods but, crucially, we do not use the estimated geometry as the final representation of the scene; instead, we use it to construct *VMem*, which is a memory of past views. We represent the scene geometry using surfels which, compared to meshes, are more robust, and, compared to point clouds, can represent occlusions. Each surfel stores in its attributes a set of indexes corresponding to past viewpoints that observed it.

To retrieve relevant past viewpoints, we render the surfels with their attributes from the novel viewpoint and splat them onto an image grid. Each pixel in the resulting image then corresponds to a set of viewpoint indexes. We select the top  $n$  most frequently represented viewpoint indexes and use them to retrieve past views from the database, where each view is represented by an RGB image and its corresponding camera parameters. A key advantage of our approach over inpainting-based methods is that it does not require highly accurate scene geometry. As long as we successfully retrieve the most relevant past views, our method remains robust.

By leveraging *Surfel-Indexed View Memory*, we significantly reduce the memory and computational burden of

conditioning on a large number of previous views, as required by multi-view/video-based methods, while improving long-term consistency across generated novel views.

Our approach represents a step toward scalable, realistic, and long-term autoregressive scene generation, making the following contributions:

1. We introduce *Surfel-Indexed View Memory*, a *plug-and-play* module to index past views geometrically and use them to condition the generation of novel views.
2. We show that our method can generate long-term coherent videos of scenes, outperform existing approaches.
3. We validate our approach on a number of challenging benchmarks, outperforming the current open-source state-of-the-art methods.

## 2. Related Work

Novel view synthesis (NVS) is a challenging and ill-posed problem. NVS methods can generally be categorized into two main approaches: view interpolation methods [3–6, 9, 20, 31, 38], which generate views that stay close to the given inputs, and view extrapolation or perpetual view generation, where novel views extend significantly beyond the original scene, often introducing large amounts of new content. The latter is particularly difficult when only a single image is available. Between these two categories lie methods focusing on single-view scene reconstruction, which have been mostly successful for scenes containing a single object [1, 13, 18, 28, 30, 39] or highly bounded scenes [29]. However, their extrapolation capabilities remain very limited. The most relevant to our work are models for single-image perpetual view generation, which typically fall into two main categories: those that incorporate explicit geometric modeling with inpainting techniques and those directly based on image or video generation.

**Inpainting-based perpetual view generation.** Inpainting-based methods [7, 12, 16, 17, 19, 22, 25, 27, 37, 42] use pre-trained 3D reconstruction methods to generate explicit 3D representations—such as meshes, point clouds, or Gaussian splats—from an initial image. These representations are reprojected into novel views, where 2D inpainting models fill in missing regions. For example, SceneScape [7] reconstructs a mesh from the first image using a pre-trained depth estimator. A diffusion-based inpainting model then completes the projected novel view, which is reprojected back to refine and extend the mesh. This process is iterated to generate additional views. MultiDiff [19] also relies on a depth estimator to warp the reference image into multiple novel views, training a diffusion model to inpaint missing regions simultaneously. CamCtrl3D [22] follows a similar approach but incorporates a ray map to better condition the diffusion model for view synthesis. ViewCrafter [42] uses a pre-trained pointmap estimator to create a 3D point cloud

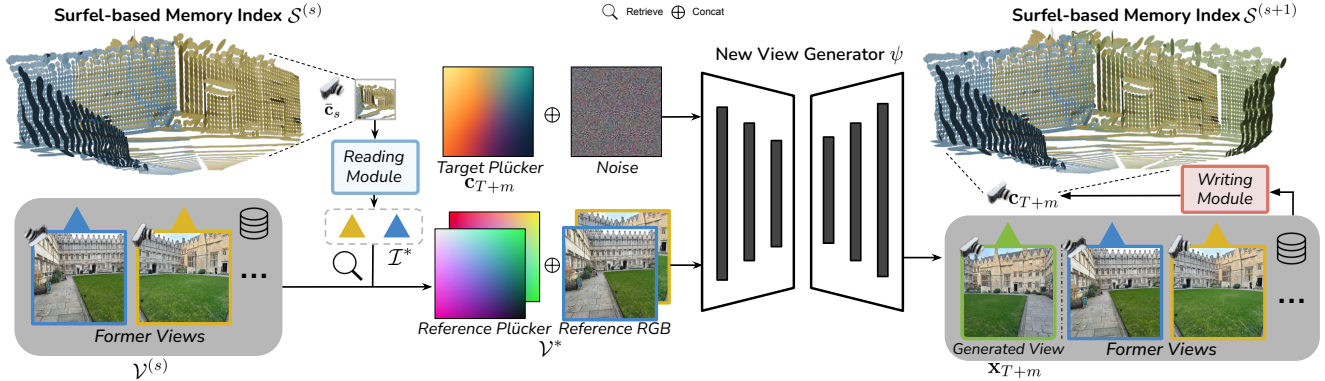


Figure 2. **Method overview.** Given novel camera viewpoints  $\{c_{T+m}\}_{m=1}^M$ , we first use our proposed memory module Surfel-Indexed View Memory  $\mathcal{V}^{(s)}$  to retrieve the most relevant  $K$  past views  $v_t \in \mathcal{V}^* \subset \mathcal{V}^{(s)}$  as conditioning reference views. For each retrieved view, the camera parameters  $c_t$  are represented using Plücker embeddings, which are spatially resized via interpolation to match the resolution of the encoded image latents. The corresponding reference images  $x_t$  are encoded using a VAE to obtain latent feature maps. These resized Plücker embeddings and VAE-encoded latents are then fed into the camera-conditioned image-set generator  $\psi$  to synthesize the novel views  $\{x_{T+m}\}_{m=1}^M$ . Once the new views are generated, we update the surfel-indexed memory  $\mathcal{S}^{(s)} \rightarrow \mathcal{S}^{(s+1)}$  by appending the new view indices  $\{T+m\}_{m=1}^M$  to existing surfels or creating new ones based on the estimated geometry of the generated views. This process is repeated autoregressively for each subsequent generation step.

and trains a video diffusion model for inpainting. GenWarp [27], uniquely, warps a 2D coordinate representation of the reference view into novel views and uses it to condition generation.

While these methods improve geometric consistency, they are highly susceptible to errors in depth or pointmap estimation, which can propagate distortions across generated views. Once the 3D representation is constructed, any inaccuracies from depth or pointmap estimation become difficult to correct. Moreover, scaling these approaches to large scenes is computationally intensive, as storing and processing explicit high-fidelity 3D representations requires substantial memory.

**Multi-view-based perpetual view generation.** Another category of methods [8, 23, 26, 32, 36, 41, 46] avoids explicitly modeling the 3D geometry of the scene. Instead, these approaches generate novel views by conditioning on previously rendered or generated views.

GeoGPT [26] establishes this direction by using an autoregressive likelihood model to synthesize novel perspectives from a single input image. Building upon this, LookOut [23] improves consistency by generating view sequences along a predefined camera trajectory, conditioning on up to two preceding views. It also incorporates a post-processing step that reuses previously generated frames as additional context for future predictions. Other methods, such as [32, 41], enhance novel view synthesis by employing cross-view attention or enforcing epipolar constraints within diffusion models. MotionCtrl [36], in particular, leverages geometric priors from a pre-trained video diffusion model to synthesize camera-controllable videos. All

of the aforementioned methods are *trajectory-based*, requiring the input views to follow a continuous spatial path. In contrast, *image-set models* like CAT3D [8] are capable of synthesizing novel views from a sparse and unordered set of input images, without any trajectory constraint. Most recently, SEVA [46] has emerged as a strong open-source alternative in this image-set modeling paradigm.

However, all these methods are computationally expensive, with an  $O(n^2)$  complexity for attention, which restricts the number of conditioning views to a small context window containing only a few of the most recently generated frames. This limitation negatively impacts the long-term consistency of the generated images.

Several concurrent works have explored memory-based approaches for consistent scene generation. StarGen [44] and WorldMem [40] use distance and field-of-view-based spatial memory retrieval, which can recover spatially correlated views but lack geometric reasoning for occlusion handling. Genie [2, 21] maintains memory through recurrent state features. Gen3C [24] conditions on stored point clouds similar to ViewCrafter [43], inheriting the limitations of inpainting-based methods. In contrast, our surfel-based memory explicitly models occlusion and provides more principled view selection.

### 3. Method

Let  $x_1 \in \mathbb{R}^{H \times W \times 3}$  be an RGB image of a scene that we wish to explore, and let  $\{c_t\}_{t=1}^T$  be a sequence of camera parameters specifying a path through the scene. Our goal is to generate a corresponding video, *i.e.*, a sequence of images  $\{x_t\}_{t=1}^T$ , where  $x_1$  is the given input image, and each

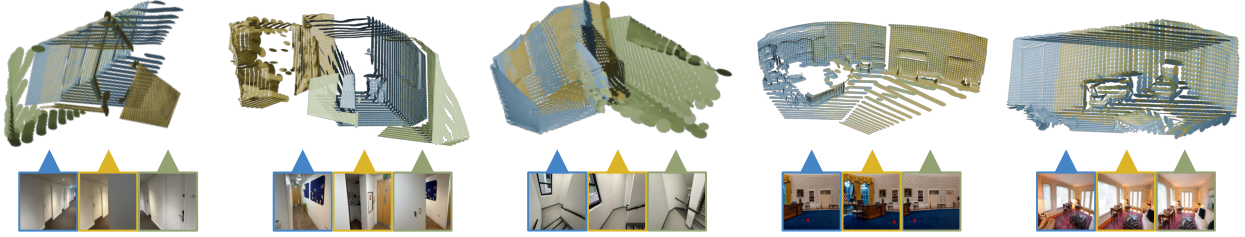


Figure 3. **Visualization of our surfel-based memory index.** Each surfel in the 3D scene stores indices of all views that have observed it. For visualization, we color-code each surfel by the indices of the contributing views. This spatial index enables efficient retrieval of relevant past views: when generating a new view, we identify which surfels are visible from the target viewpoint and retrieve the views that previously observed those same regions, naturally accounting for occlusion.

subsequent frame  $\mathbf{x}_t$  is consistent with the previous ones and reflects the specified camera  $\mathbf{c}_t$ . Moreover, we aim to do so autoregressively, generating  $M$  novel views at a time for the given cameras (with  $M$  kept small to ensure interactivity) while ensuring consistency with previously generated views. This enables interactive scene exploration, where the user can specify the next camera positions at each step.

We define a *view* as a tuple  $v_t = (\mathbf{x}_t, \mathbf{c}_t)$  consisting of an image  $\mathbf{x}_t$  and its corresponding camera  $\mathbf{c}_t$  at timestep  $t$ . At generation step  $s$ , we have generated  $T = sM$ ,  $s \geq 0$  frames so far. The goal is to generate  $M$  new RGB images  $\{\mathbf{x}_{T+m}\}_{m=1}^M$  for the next target camera parameters  $\{\mathbf{c}_{T+m}\}_{m=1}^M$ , given the previously generated views  $\mathcal{V}^{(s)} = \{v_1, v_2, \dots, v_T\}$ . After generation, we update  $T \leftarrow T + M$ .

A challenge with this approach is that the context  $\mathcal{V}^{(s)}$  grows unbounded over time. Video generators addressing this problem [23, 26, 36, 41] typically consider a fixed-length subset of  $\mathcal{V}^{(s)}$ , conditioning their generation only on the most recent  $L$  views  $\{v_{T-L+1}, \dots, v_T\}$ . This limitation results in severe inconsistencies when the generated sequence extends beyond the (small) context window.

We solve this problem by dynamically retrieving the most relevant subset of past views, denoted as  $\mathcal{V}^* \subseteq \mathcal{V}^{(s)}$ . To achieve this, we introduce an efficient data structure, the Surfel-Indexed View Memory, that stores and retrieves past views based on their approximate 3D geometry. We first describe the Surfel-Indexed View Memory (Sec. 3.1) and then introduce the novel view generator (Sec. 3.2). An overview of the method is provided in Fig. 2.

### 3.1. Surfel-Indexed View Memory

Consider the problem of generating the next views  $\{\mathbf{x}_{T+m}\}_{m=1}^M$  of the scene as seen from the cameras  $\{\mathbf{c}_{T+m}\}_{m=1}^M$ . The generator must consider the previously generated views and ensure  $\{\mathbf{x}_{T+m}\}_{m=1}^M$  are consistent with those, while generating new content as needed. However, not all past views are equally correlated with the novel views  $\{\mathbf{x}_{T+m}\}_{m=1}^M$ . We prioritize past views that have likely observed the largest portion of the scene currently

being generated. For example, if the current locale is surrounded by walls, parts of the scene behind those walls are likely less relevant for generating a new view of that locale. Conversely, views that share a similar visible region with the target view can provide more useful information for generating its content.

This principle drives our design for a view memory mechanism. We maintain a coarse model of the scene geometry using surfels (visualized in Fig. 3), simple surface primitives that account for occlusion. Each surfel stores the indices of the past views that observed it. To generate a new view, the surfels visible from the new viewpoint are retrieved, using the associated indices to vote for which views to consider for generation. This process is illustrated in Fig. 4.

Specifically, we define a *surfel* as the tuple

$$\mathbf{s}_k = (\mathbf{p}_k, \mathbf{n}_k, r_k, \mathcal{I}_k),$$

where  $\mathbf{p}_k \in \mathbb{R}^3$  denotes the surfel’s 3D position,  $\mathbf{n}_k \in \mathbb{R}^3$  is its surface normal,  $r_k \in \mathbb{R}$  is the surfel radius, and  $\mathcal{I}_k \subseteq \{1, 2, \dots, T\}$  is a subset of past view indices that observed the surfel. The surfel-based memory indexing of past views  $\mathcal{V}^{(s)}$ , encapsulating the scene, is represented as a set of surfels  $\mathcal{S}^{(s)} = \{\mathbf{s}_k\}_{k=1}^{N^{(s)}}$ , where  $N^{(s)}$  is the number of surfels at generation step  $s$ . We also maintain an octree to quickly retrieve surfels based on their geometry. Next, we describe how to read from and write to this memory.

**Reading from the memory.** To retrieve the most relevant past views from the memory  $\mathcal{V}^{(s)}$  for the novel cameras  $\{\mathbf{c}_{T+m}\}_{m=1}^M$ , we first compute their average pose  $\bar{\mathbf{c}}_s \in \text{SE}(3)$  as a reference (refer to Appendix A). Then we render the surfels  $\mathcal{S}^{(s)}$  from the averaged camera pose  $\bar{\mathbf{c}}_s$ . Each surfel is rendered as a splat with its attributes, accounting for relative depth and occlusions, and contributing to the image based on its coverage. The rendered attributes correspond to the indices of the previous views. The core intuition is that views observing the largest portion of the scene from the perspective of the novel camera are most relevant for novel view synthesis. To identify these views, we rank

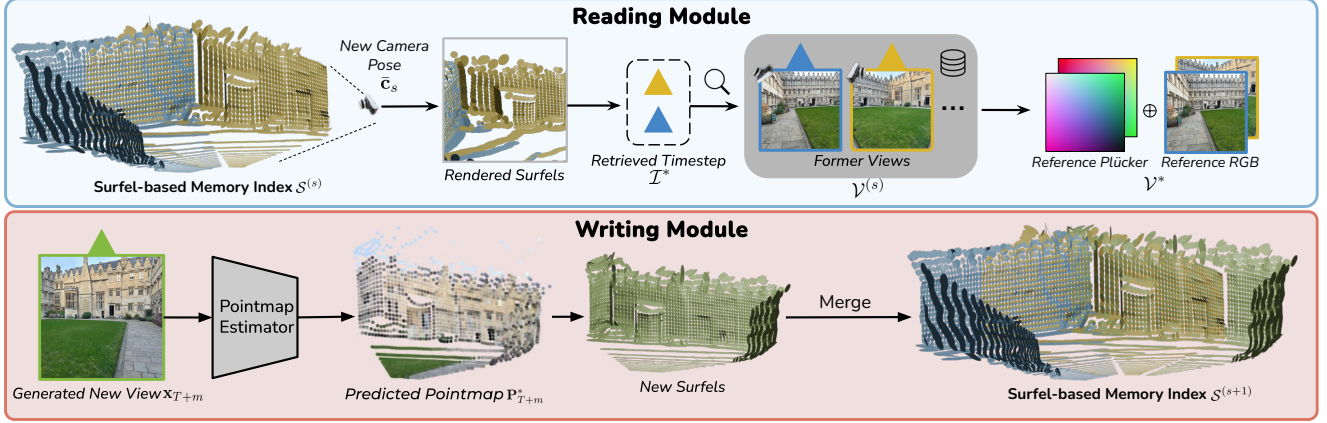


Figure 4. **Surfel-Indexed View Memory.** *Reading* from the memory involves rendering the surfels  $\mathcal{S}^{(s)}$  along with their attributes, which contain past view indices represented by frame indices. We then select the  $K$  most frequently represented frame indices in the rendered image to retrieve the most relevant past views from  $\mathcal{V}^{(s)}$ . *Writing* to the memory involves estimating the geometry of the newly generated views  $\{\mathbf{x}_{T+m}\}_{m=1}^M$  in the form of surfels and merging them with the existing surfels. The frame indices  $\{T+m\}_{m=1}^M$  are appended to the surfels observed in these views, and the novel views are stored in memory, updating  $\mathcal{V}^{(s)} \rightarrow \mathcal{V}^{(s+1)}$  and  $\mathcal{S}^{(s)} \rightarrow \mathcal{S}^{(s+1)}$ .

past view indices based on their frequency across all rendered pixels.

We then select the top- $K$  most frequently represented indices  $\mathcal{I}^*$  and use them to retrieve the corresponding past views,  $\mathcal{V}^* = \{v_t\}_{t \in \mathcal{I}^*}$ , from the memory  $\mathcal{V}^{(s)}$ . This subset of views is used to feed the new view generator, as described in Sec. 3.2.

To avoid oversampling repeatedly visited regions, we apply a non-maximum suppression algorithm that reduces redundancy in memory and promotes broader scene coverage among the top- $K$  views. During retrieval, we retain only the most frequently referenced view among those with similar poses. Additionally, during writing to the memory, we merge surfels by comparing their associated camera poses—if two poses are highly similar, we discard the older one.

**Writing to the memory.** After generating the new views  $\{v_{T+m} = (\mathbf{x}_{T+m}, \mathbf{c}_{T+m})\}_{m=1}^M$ , we add them to the memory  $\mathcal{V}^{(s)}$  and update the surfel-based memory index  $\mathcal{S}^{(s)}$ . We use an off-the-shelf point map estimator  $\phi$ , such as CUT3R [33], to output their corresponding point maps  $\{\mathbf{P}_{T+m}^*\}_{m=1}^M$ . Specifically, we jointly estimate the point maps for the newly generated views along with the retrieved past views  $\mathcal{V}^*$ . This joint estimation ensures that the new point maps are aligned with the coordinate frame of the existing scene geometry in the surfel-based memory index  $\mathcal{S}^{(s)}$ .

Next, we convert the estimated point maps to a set of new surfels. For each newly generated frame  $t \in \{T+1, T+2, \dots, T+M\}$ , we process its point map  $\mathbf{P}_t^*$ . Since our approach only requires coarse geometry, we first downsample the point map  $\mathbf{P}_t^*$  by a factor  $\sigma$ , yielding a smaller point map

$\mathbf{P}_t \in \mathbb{R}^{H' \times W' \times 3}$ , where  $H' = H/\sigma$  and  $W' = W/\sigma$ . For each pixel location  $(u, v)$  in the downsampled point map, we have a 3D point  $\mathbf{p}_{u,v,t}$ , and we create a new surfel  $\mathbf{s}_{k'}$  centered on it. We compute each surfel’s normal using the cross-product of displacement vectors to neighboring pixels. For a pixel at 2D location  $(u, v)$  in the image grid, we use neighboring pixels to estimate the local surface normal:

$$\mathbf{n}_{k'} = \frac{(\mathbf{p}_{u+1,v,t} - \mathbf{p}_{u-1,v,t}) \times (\mathbf{p}_{u,v+1,t} - \mathbf{p}_{u,v-1,t})}{\|(\mathbf{p}_{u+1,v,t} - \mathbf{p}_{u-1,v,t}) \times (\mathbf{p}_{u,v+1,t} - \mathbf{p}_{u,v-1,t})\|},$$

where  $\mathbf{p}_{u,v,t}$  represents the 3D point at image coordinates  $(u, v)$  in frame  $t$ . To ensure that the surfels reasonably cover the scene, we use a heuristic to compute the surfel’s radius, which is proportional to the depth of the surfel and inversely proportional to the focal length and the cosine of the angle between the surfel normal and the viewing direction:

$$r_{k'} = \frac{\frac{1}{2} \mathbf{D}_{u,v,t} / f_t}{\alpha + (1 - \alpha) \|\mathbf{n}_{k'} \cdot (\mathbf{p}_{u,v,t} - \mathbf{O}_t)\|},$$

where  $\mathbf{D}_{u,v,t}$  represents the depth at pixel  $(u, v)$  in frame  $t$ ,  $\mathbf{O}_t$  is the camera center of frame  $t$ ,  $\mathbf{p}_{u,v,t} - \mathbf{O}_t$  is the viewing direction, and  $f_t$  is the focal length at time  $t$ . The factor  $\alpha$  is used to avoid extreme values when  $\|\mathbf{n}_{k'} \cdot (\mathbf{p}_{u,v,t} - \mathbf{O}_t)\| \approx 0$ .

Finally, we check if the index  $\mathcal{S}^{(s)}$  already contains a surfel  $\mathbf{s}_k$  similar to the new surfel  $\mathbf{s}_{k'}$ . Two surfels match if their centers are within a distance  $d$  and the cosine similarity between their normals is above a threshold  $\theta$ . If such a surfel  $\mathbf{s}_k$  is found, we add the frame index  $t$  to the surfel’s set of past view indices:  $\mathcal{I}_k \leftarrow \mathcal{I}_k \cup \{t\}$ , and discard  $\mathbf{s}_{k'}$ . If not, we set  $\mathcal{I}_{k'} = \{t\}$  and add  $\mathbf{s}_{k'}$  to the index  $\mathcal{S}^{(s+1)}$ . This process transforms the surfel memory from  $\mathcal{S}^{(s)}$  to  $\mathcal{S}^{(s+1)}$  with  $N^{(s+1)}$  surfels for the next generation step.

### 3.2. Novel View Generator

We use a camera-conditioned image-set generator  $\psi$  to generate new views. The generator  $\psi$  takes  $K$  retrieved reference views  $\mathcal{V}^* = \{v_t = (\mathbf{x}_t, \mathbf{c}_t)\}_{t \in \mathcal{I}^*}$  and the target camera poses  $\{\mathbf{c}_{T+m}\}_{m=1}^M$  for the  $M$  new frames to be generated and samples the new views:

$$\{\mathbf{x}_{T+m}\}_{m=1}^M \sim \psi(\{(\mathbf{x}_t, \mathbf{c}_t)\}_{t \in \mathcal{I}^*}, \{\mathbf{c}_{T+m}\}_{m=1}^M),$$

where  $\mathcal{I}^* \subseteq \{1, 2, \dots, T\}$  are the frame indices of the retrieved reference views.

Specifically, we base our generator on the recently released pre-trained SEVA [46] model. Given the plug-and-play nature of our memory module, VMem can work with other image-set generators as well. While our model can operate with SEVA out-of-the-box, the original SEVA is trained with a large fixed total number of reference and target frames ( $K + M = 21$ ), which demands substantial computational resources that may be prohibitive for many applications. To address this, we fine-tune a more efficient version that operates with a reduced number of reference frames ( $K = 4$ ) and target views ( $M = 4$ ) and use it for our main experiments. Our ablation studies (Sec. 4.6) demonstrate that this fine-tuned version, when combined with VMem, achieves comparable performance to the original SEVA while delivering approximately  $10\times$  speedup at inference time.

## 4. Experiments

We conduct experiments on long-term, short-term, and cycle-trajectory perpetual view generation tasks, comparing our models to previous open-source single-view approaches. Our results show that VMem can generate more coherent long-term scenes and demonstrates significantly better camera control than all existing open-source video generation methods.

### 4.1. Implementation Details

The novel view generator of VMem is trained on the RealEstate10K dataset [47] using SEVA [46] as a pretrained backbone. The number of context views  $K$  is set to 4, and the number of target views  $M$  is also 4. We randomly sample context views online during training. We use LoRA [14] with rank 256 to fine-tune the base model. The model is trained for 600,000 iterations on 8 A40 GPUs, with a batch size of 24 per GPU. The model is optimized using AdamW with a learning rate of  $3 \times 10^{-6}$ , a weight decay of  $10^{-4}$ , and a cosine annealing schedule. During inference, the classifier-free guidance scale is set to 3. The scaling factor  $\sigma$  for the point map is set to 0.03, and  $\alpha$  is set to 0.2 in the surfel radius calculation.

### 4.2. Evaluation Metrics

We evaluate the quality of generated novel views based on three key factors: (1) the overall quality of generated novel views, (2) the model’s ability to preserve input image details across views, and (3) the alignment between generated camera poses and ground truth.

For (1), we compare the distribution of the generated novel views to that of the test set using Fréchet Image Distance (FID) [11]. For (2), we measure peak signal-to-noise ratio (PSNR) for pixel differences, along with LPIPS [45] and SSIM [35], as done in [23]. For (3), following [10], we express each estimated camera pose relative to the first frame and normalize the translation by the furthest frame. We use DUST3R [34] to extract poses from generated views. We then calculate the rotation distance  $R_{\text{dist}}$  by comparing the the ground truth and extracted rotation matrices of each generated novel view sequence, expressed as:

$$R_{\text{dist}} = \arccos\left(\frac{\text{tr}(\mathbf{R}_{\text{gen}} \cdot \mathbf{R}_{\text{gt}}^T) - 1}{2}\right),$$

where  $\mathbf{R}$  denotes a rotation matrix. We also compute the translation distance  $t_{\text{dist}}$  as:

$$t_{\text{dist}} = \|\mathbf{t}_{\text{gt}} - \mathbf{t}_{\text{gen}}\|_2.$$

### 4.3. Datasets and Evaluation Settings

We consider two real-world datasets for new view synthesis evaluation: RealEstate10K [47] and Tanks-and-Temples [15]. RealEstate10K comprises video clips of indoor scenes. We use the training split of RealEstate10K to train VMem. For evaluation, following [23, 41], we only consider test sequences with at least 200 frames. Starting from the first frame of the ground truth test sequence, we generate 20 images using 20 camera poses along the ground truth trajectory, spaced ten frames apart, with the final pose 200 frames from the initial view. Short-term evaluations use the fifth generated image, while long-term evaluations focus on the final image. For cycle evaluation, each model generates frames from the initial to the final camera pose and then back to the start, with evaluations conducted only on the return trajectory. The goal of this evaluation is to test the model’s ability to maintain scene consistency when revisiting previously traversed paths. For Tanks-and-Temples, which includes out-of-domain indoor and outdoor scenes featuring much larger motion speeds, we use all six advanced scenes and evaluate cycle-trajectory settings for the first 50 frames without skipping frames.

### 4.4. Cycle-Trajectory Perpetual View Generation

The key advantage of VMem is its ability to remember previously generated content across different locations, as demonstrated by the cycle-trajectory setting. VMem surpasses all baseline methods on both in-domain (Tab. 2) and

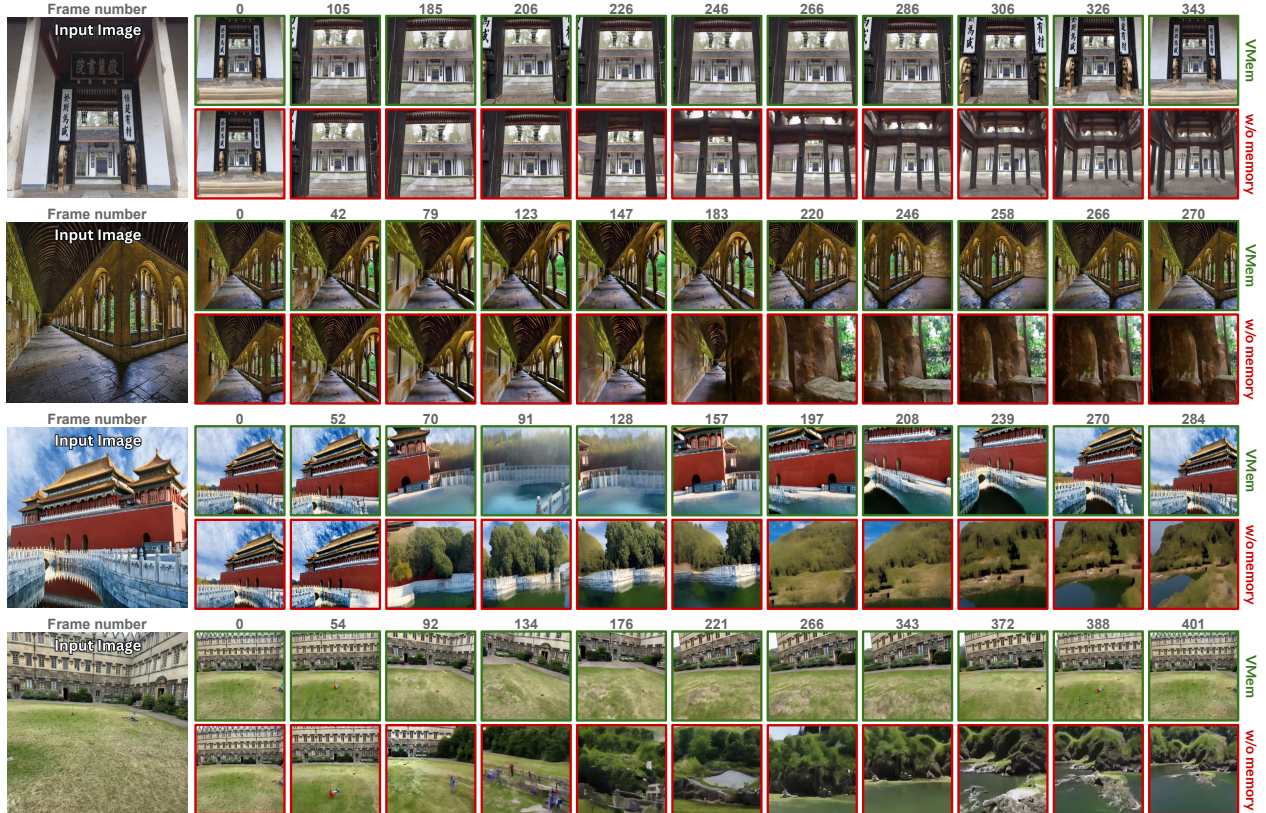


Figure 5. **Generalization to long sequences with revisitations.** We compare scene generation with and without our proposed memory module (VMem). For each sequence, an input image is shown on the left, followed by generated frames at selected frame indices. Our method (top row in each pair) maintains high spatial consistency across revisited viewpoints, while the baseline without memory (bottom row) suffers from visual drift and structural degradation over time.

	Short-term ( $50^{th}$ frame)						Long-term ( $> 200^{th}$ frame)					
	LPIPS ↓	PSNR ↑	SSIM ↑	FID ↓	$R_{dist}$ ↓	$T_{dist}$ ↓	LPIPS ↓	PSNR ↑	SSIM ↑	FID ↓	$R_{dist}$ ↓	$T_{dist}$ ↓
GeoGPT [26]	0.444	13.35	–	26.72	–	–	0.674	9.54	–	41.87	–	–
Lookout [23]	0.378	14.43	–	28.86	1.241	0.876	0.658	10.51	–	58.12	1.142	0.924
PhotoNVS [41]	0.333	15.51	–	21.76	–	–	0.588	11.54	–	41.95	–	–
GenWarp [27]	0.436	12.03	0.144	29.69	0.564	0.059	0.613	9.56	0.085	36.40	0.850	<b>0.251</b>
MotionCtrl [36]	0.424	12.00	0.148	19.25	0.341	0.356	0.605	9.13	0.083	35.45	<b>0.748</b>	0.609
ViewCrafter [42]	0.377	16.97	0.262	25.39	1.562	0.208	0.592	9.74	0.148	34.12	2.177	0.827
VMem	<b>0.287</b>	<b>18.49</b>	<b>0.406</b>	<b>17.12</b>	<b>0.219</b>	<b>0.039</b>	<b>0.493</b>	<b>13.12</b>	<b>0.183</b>	<b>27.15</b>	0.811	0.499

Table 1. **Quantitative single-view NVS comparison on RealEstate10K** Lower is better for LPIPS, FID,  $R_{dist}$ ,  $T_{dist}$ ; higher is better for PSNR, SSIM. VMem surpasses all baseline methods on this benchmark, but its **true advantage—spatial consistency—is not fully reflected**, as the trajectories in RealEstate10K rarely revisit previously observed areas.

out-of-domain (Tab. 3) benchmarks. Additionally, qualitative comparisons in Fig. 6 clearly illustrate that VMem can generate realistic content in unseen regions with significantly more precise camera control than both inpainting-based and multi-view/video-based baselines. Furthermore, VMem preserves the memory of previously generated frames, ensuring scene consistency upon revisiting previous locations—an ability that none of the multi-view/video-based baseline methods possess.

#### 4.5. Long- and Short-Term Perpetual View Generation

To further validate our approach, we evaluate VMem on the widely recognized benchmark established in [23, 41] for both short-term and long-term perpetual generation tasks. As demonstrated in Tab. 1, VMem substantially outperforms all baseline methods across all metrics, achieving superior scene extrapolation and significantly improved cam-

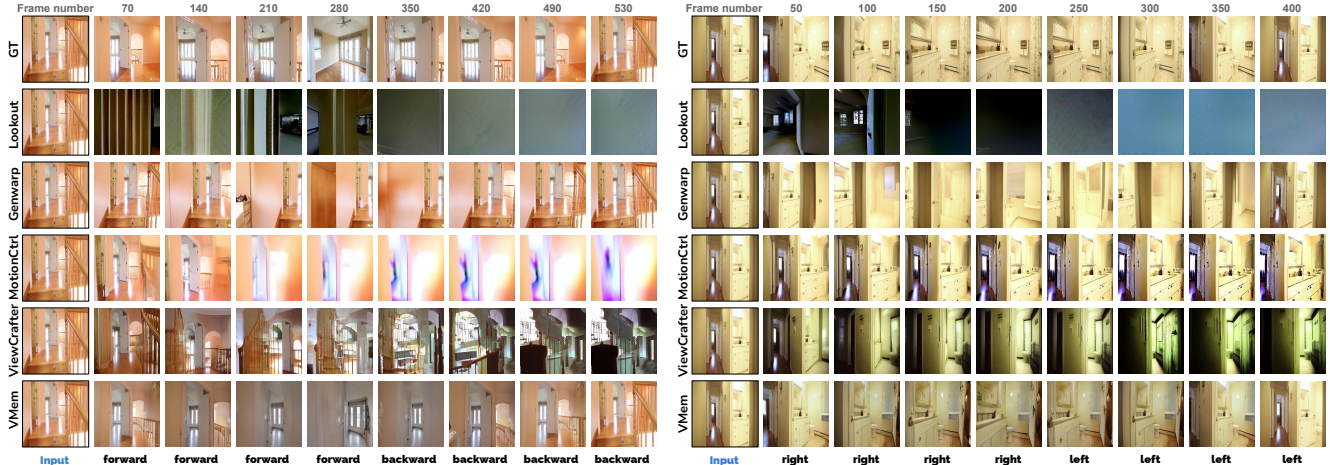


Figure 6. **Qualitative comparison of the cycle trajectory frames** ( $> 400$  frames). Under the cycle trajectory setting, VMem can realistically infer and generate unseen content with significantly more precise camera control than both inpainting-based and multi-view/video-based baseline methods. Moreover, it retains memory of all previously generated frames, ensuring consistency when revisiting locations—an ability none of the multi-view/video-based baseline methods [23, 36, 42] possess.

Method	LPIPS ↓	PSNR ↑	SSIM ↑	FID ↓	$R_{\text{dist}}$ ↓	$T_{\text{dist}}$ ↓
Look-out [23]	0.809	8.41	0.069	38.34	1.262	0.341
GenWarp [27]	0.507	11.13	0.134	32.94	0.848	0.241
MotionCtrl [36]	0.589	9.07	0.096	26.86	0.871	0.293
ViewCrafter [42]	0.401	11.82	0.217	24.72	0.902	0.492
VMem	<b>0.381</b>	<b>14.82</b>	<b>0.275</b>	<b>24.97</b>	<b>0.793</b>	<b>0.124</b>

Table 2. **Quantitative comparison on cycle trajectories from RealEstate10K.** LPIPS (lower is better), PSNR (higher is better),  $R_{\text{dist}}$  (lower is better),  $T_{\text{dist}}$  (lower is better).

Method	LPIPS ↓	PSNR ↑	SSIM ↑	$R_{\text{dist}}$ ↓	$T_{\text{dist}}$ ↓
Look-out [23]	0.792	8.52	0.008	<b>0.727</b>	1.499
GenWarp [27]	0.521	10.27	<b>0.129</b>	0.785	1.982
MotionCtrl [36]	0.692	8.21	0.082	0.842	<b>0.129</b>
ViewCrafter [42]	0.494	13.62	<b>0.129</b>	1.643	0.492
VMem	<b>0.472</b>	<b>14.11</b>	0.121	1.204	0.387

Table 3. **Quantitative comparison on cycle trajectories from Tanks and Temples.** LPIPS (lower is better), PSNR (higher is better), SSIM (higher is better),  $R_{\text{dist}}$  (lower is better),  $T_{\text{dist}}$  (lower is better).

era control. These quantitative improvements are further supported by qualitative comparisons in Fig. 6. Notably, VMem enables the generation of consistent, high-quality long videos of scenes across diverse scenarios beyond those in RealEstate10K, as shown in Fig. 5. We believe this represents a crucial step forward in advancing the creation of immersive virtual worlds.

#### 4.6. Ablation Study

We conduct an ablation study to assess the effectiveness of our proposed surfel-based memory indexing for context

Context views $K$	View Retrieval	LPIPS ↓	PSNR ↑	SSIM ↑	$R_{\text{dist}}$ ↓	$T_{\text{dist}}$ ↓
17	Temporal	0.477	13.92	0.188	0.976	0.254
	Camera Distance (SEVA [46])	0.397	15.72	0.297	<b>0.821</b>	0.392
	Field of View	0.374	15.75	0.292	0.911	0.382
	VMem	<b>0.304</b>	<b>18.15</b>	<b>0.377</b>	0.892	<b>0.165</b>
4	Temporal	0.794	7.52	0.018	1.942	0.458
	Camera Distance	0.422	13.27	0.187	1.787	0.319
	Field of View	0.424	13.11	0.192	1.782	0.285
	VMem	<b>0.381</b>	<b>14.82</b>	<b>0.275</b>	<b>0.793</b>	<b>0.124</b>

Table 4. **Ablation study on cycle trajectories from RealEstate10K.** We compare different view retrieval strategies for two context view counts  $K$ .  $K = 17$  is the maximum context size in SEVA [46] for generating  $M = 4$  target views, while we use  $K = 4$  in our main experiments due to the  $\sim 12\times$  faster inference. The original SEVA strategy relies on camera distance for retrieval.

view retrieval in VMem. Specifically, we evaluate our approach in the cycle-trajectory setting and compare it against alternative view retrieval strategies: temporal-based, camera distance-based, and field of view-based retrieval. For temporal-based retrieval, we select the most recent  $K$  views from memory. For camera distance-based retrieval, we select the top  $K$  views with cameras closest to the target view camera—this strategy is also employed by SEVA [46], which serves as our backbone novel view generator. For field of view-based retrieval, we select the top  $K$  views with the highest field of view overlap with the target view.

We also evaluate the performance trade-off between our lightweight, fine-tuned novel view generator using  $K = 4$  context views versus the original SEVA configuration with  $K = 17$  context views. The results are reported in Tab. 4.

Our findings demonstrate that VMem consistently improves the performance of the novel view generator across

both context view configurations. The improvement is most pronounced when using fewer context views ( $K = 4$ ), highlighting the effectiveness of our surfel-based memory indexing.

Notably, our VMem with only  $K = 4$  views recovers most of the performance achieved with  $K = 17$  views in the original SEVA setting while delivering approximately  $12\times$  speed improvement. On an RTX 4090 GPU, our lightweight novel view generator takes 4.2 seconds per frame, while the original SEVA takes 50 seconds per frame.

## 5. Conclusion

We introduced *Surfel-Indexed View Memory (VMem)*, a novel plug-and-play memory mechanism for long-term autoregressive scene generation using a surfel-indexed view memory. By anchoring past views to a surfel-based representation of the scene and retrieving the most relevant ones, our approach improves long-term scene consistency while reducing computational costs. Experiments on long-term scene synthesis benchmarks demonstrate that *VMem* outperforms existing methods in coherence and image quality. Our work advances scalable video generation with applications in virtual reality, gaming, and other domains.

**Acknowledgments.** The authors of this work are supported by Clarendon scholarship, ERC 101001212-UNION, and AIMS EP/S024050/1. The authors would like to thank Xingyi Yang, Zeren Jiang, Junlin Han, Zhongrui Gui for their insightful feedback.

## References

- [1] Mark Boss, Zixuan Huang, Aaryaman Vasishtha, and Varun Jampani. SF3D: Stable fast 3D mesh reconstruction with uv-unwrapping and illumination disentanglement. *arXiv preprint arXiv:2408.00653*, 2024. 2
- [2] Jake Bruce, Michael D Dennis, Ashley Edwards, Jack Parker-Holder, Yuge Shi, Edward Hughes, Matthew Lai, Aditi Mavalankar, Richie Steigerwald, Chris Apps, et al. Genie: Generative interactive environments. In *Forty-first International Conference on Machine Learning*, 2024. 3
- [3] Anpei Chen, Zexiang Xu, Fuqiang Zhao, Xiaoshuai Zhang, Fanbo Xiang, Jingyi Yu, and Hao Su. Mvsnerf: Fast generalizable radiance field reconstruction from multi-view stereo. In *Proceedings of the IEEE/CVF international conference on computer vision*, pages 14124–14133, 2021. 2
- [4] Hansheng Chen, Jiatao Gu, Anpei Chen, Wei Tian, Zhuowen Tu, Lingjie Liu, and Hao Su. Single-Stage Diffusion NeRF: A Unified Approach to 3D Generation and Reconstruction, 2023. arXiv:2304.06714 [cs].
- [5] Yuedong Chen, Haofei Xu, Chuanxia Zheng, Bohan Zhuang, Marc Pollefeys, Andreas Geiger, Tat-Jen Cham, and Jianfei Cai. Mvsplat: Efficient 3d gaussian splatting from sparse multi-view images. *arXiv preprint arXiv:2403.14627*, 2024.
- [6] Yuedong Chen, Chuanxia Zheng, Haofei Xu, Bohan Zhuang, Andrea Vedaldi, Tat-Jen Cham, and Jianfei Cai. Mvsplat360: Feed-forward 360 scene synthesis from sparse views. 2024. 2
- [7] Rafail Fridman, Amit Abecasis, Yoni Kasten, and Tali Dekel. Scenescape: Text-driven consistent scene generation. *arXiv preprint arXiv:2302.01133*, 2023. 1, 2
- [8] Ruiqi Gao, Aleksander Holynski, Philipp Henzler, Arthur Brussee, Ricardo Martin-Brualla, Pratul Srinivasan, Jonathan T. Barron, and Ben Poole. CAT3D: create anything in 3d with multi-view diffusion models. *arXiv*, 2405.10314, 2024. 3
- [9] Ruiqi Gao\*, Aleksander Holynski\*, Philipp Henzler, Arthur Brussee, Ricardo Martin-Brualla, Pratul P. Srinivasan, Jonathan T. Barron, and Ben Poole\*. Cat3d: Create anything in 3d with multi-view diffusion models. *Advances in Neural Information Processing Systems*, 2024. 2
- [10] Hao He, Yinghao Xu, Yuwei Guo, Gordon Wetzstein, Bo Dai, Hongsheng Li, and Ceyuan Yang. Cameractrl: Enabling camera control for text-to-video generation. *arXiv preprint arXiv:2404.02101*, 2024. 6
- [11] Martin Heusel, Hubert Ramsauer, Thomas Unterthiner, Bernhard Nessler, and Sepp Hochreiter. Gans trained by a two time-scale update rule converge to a local nash equilibrium. *Advances in neural information processing systems*, 30, 2017. 6
- [12] Lukas Höllein, Ang Cao, Andrew Owens, Justin Johnson, and Matthias Nießner. Text2room: Extracting textured 3d meshes from 2d text-to-image models. In *Proceedings of the IEEE/CVF International Conference on Computer Vision (ICCV)*, pages 7909–7920, 2023. 1, 2
- [13] Yicong Hong, Kai Zhang, Jiuxiang Gu, Sai Bi, Yang Zhou, Difan Liu, Feng Liu, Kalyan Sunkavalli, Trung Bui, and Hao Tan. LRM: Large reconstruction model for single image to 3D. In *Proc. ICLR*, 2024. 2
- [14] Edward J. Hu, Yelong Shen, Phillip Wallis, Zeyuan Allen-Zhu, Yuanzhi Li, Shean Wang, Lu Wang, and Weizhu Chen. LoRA: Low-rank adaptation of large language models. In *Proc. ICLR*, 2022. 6
- [15] Arno Knapitsch, Jaesik Park, Qian-Yi Zhou, and Vladlen Koltun. Tanks and temples: Benchmarking large-scale scene reconstruction. *ACM Transactions on Graphics (ToG)*, 36(4):1–13, 2017. 6
- [16] Jing Yu Koh, Harsh Agrawal, Dhruv Batra, Richard Tucker, Austin Waters, Honglak Lee, Yinfei Yang, Jason Baldrige, and Peter Anderson. Simple and effective synthesis of indoor 3d scenes. In *Proceedings of the AAAI Conference on Artificial Intelligence*, pages 1169–1178, 2023. 1, 2
- [17] Andrew Liu, Richard Tucker, Varun Jampani, Ameesh Makadia, Noah Snively, and Angjoo Kanazawa. Infinite nature: Perpetual view generation of natural scenes from a single image. In *Proceedings of the IEEE/CVF International Conference on Computer Vision*, pages 14458–14467, 2021. 1, 2
- [18] Luke Melas-Kyriazi, Christian Rupprecht, Iro Laina, and Andrea Vedaldi. RealFusion: 360 reconstruction of any object from a single image. In *Proceedings of the IEEE Conference on Computer Vision and Pattern Recognition (CVPR)*, 2023. 2

- [19] Norman Müller, Katja Schwarz, Barbara Rössle, Lorenzo Porzi, Samuel Rota Bulò, Matthias Nießner, and Peter Kotschieder. Multidiff: Consistent novel view synthesis from a single image. In *Proceedings of the IEEE/CVF Conference on Computer Vision and Pattern Recognition*, pages 10258–10268, 2024. 1, 2
- [20] Michael Niemeyer, Jonathan T Barron, Ben Mildenhall, Mehdi SM Sajjadi, Andreas Geiger, and Noha Radwan. Regnerf: Regularizing neural radiance fields for view synthesis from sparse inputs. In *Proceedings of the IEEE/CVF conference on computer vision and pattern recognition*, pages 5480–5490, 2022. 2
- [21] Jack Parker-Holder, Philip Ball, Jake Bruce, Vibhavari Dasagi, Kristian Holsheimer, Christos Kaplanis, Alexandre Moufarek, Guy Scully, Jeremy Shar, Jimmy Shi, Stephen Spencer, Jessica Yung, Michael Dennis, Sultan Kenjeyev, Shangbang Long, Vlad Mnih, Harris Chan, Maxime Gazeau, Bonnie Li, Fabio Pardo, Luyu Wang, Lei Zhang, Frederic Besse, Tim Harley, Anna Mitenkova, Jane Wang, Jeff Clune, Demis Hassabis, Raia Hadsell, Adrian Bolton, Satinder Singh, and Tim Rocktäschel. Genie 2: A large-scale foundation world model, 2024. 1, 2, 3
- [22] Stefan Popov, Amit Raj, Michael Krainin, Yuanzhen Li, William T. Freeman, and Michael Rubinstein. Camctrl3d: Single-image scene exploration with precise 3d camera control, 2025. 1, 2
- [23] Xuanchi Ren and Xiaolong Wang. Look outside the room: Synthesizing a consistent long-term 3d scene video from a single image. In *Proceedings of the IEEE/CVF Conference on Computer Vision and Pattern Recognition*, pages 3563–3573, 2022. 2, 3, 4, 6, 7, 8
- [24] Xuanchi Ren, Tianchang Shen, Jiahui Huang, Huan Ling, Yifan Lu, Merlin Nimier-David, Thomas Müller, Alexander Keller, Sanja Fidler, and Jun Gao. Gen3c: 3d-informed world-consistent video generation with precise camera control. In *Proceedings of the IEEE/CVF Conference on Computer Vision and Pattern Recognition*, 2025. 3
- [25] Chris Rockwell, David F Fouhey, and Justin Johnson. Pixel-synth: Generating a 3d-consistent experience from a single image. In *Proceedings of the IEEE/CVF International Conference on Computer Vision*, pages 14104–14113, 2021. 1, 2
- [26] Robin Rombach, Patrick Esser, and Björn Ommer. Geometry-free view synthesis: Transformers and no 3d priors. In *Proceedings of the IEEE/CVF International Conference on Computer Vision (ICCV)*, pages 14356–14366, 2021. 2, 3, 4, 7
- [27] Junyoung Seo, Kazumi Fukuda, Takashi Shibuya, Takuya Narihira, Naoki Murata, Shoukang Hu, Chieh-Hsin Lai, Seungryong Kim, and Yuki Mitsufuji. Genwarp: Single image to novel views with semantic-preserving generative warping. *arXiv preprint arXiv:2405.17251*, 2024. 1, 2, 3, 7, 8
- [28] Ruoxi Shi, Hansheng Chen, Zhuoyang Zhang, Minghua Liu, Chao Xu, Xinyue Wei, Linghao Chen, Chong Zeng, and Hao Su. Zero123++: a single image to consistent multi-view diffusion base model. *arXiv.cs, abs/2310.15110*, 2023. 2
- [29] Stanislaw Szymanowicz, Eldar Insafutdinov, Chuanxia Zheng, Dylan Campbell, Joao Henriques, Christian Ruppert, and Andrea Vedaldi. Flash3d: Feed-forward generalisable 3d scene reconstruction from a single image. *arxiv*, 2024. 2
- [30] Stanislaw Szymanowicz, Christian Ruppert, and Andrea Vedaldi. Splatter Image: Ultra-fast single-view 3D reconstruction. In *Proceedings of the IEEE Conference on Computer Vision and Pattern Recognition (CVPR)*, 2024. 2
- [31] Prune Truong, Marie-Julie Rakotosaona, Fabian Manhardt, and Federico Tombari. Sparf: Neural radiance fields from sparse and noisy poses. In *Proceedings of the IEEE/CVF Conference on Computer Vision and Pattern Recognition*, pages 4190–4200, 2023. 2
- [32] Hung-Yu Tseng, Qinbo Li, Changil Kim, Suhub Alsisan, Jia-Bin Huang, and Johannes Kopf. Consistent view synthesis with pose-guided diffusion models. In *Proceedings of the IEEE/CVF Conference on Computer Vision and Pattern Recognition*, pages 16773–16783, 2023. 3
- [33] Qianqian Wang\*, Yifei Zhang\*, Aleksander Holynski, Alexei A. Efros, and Angjoo Kanazawa. Continuous 3d perception model with persistent state. In *CVPR*, 2025. 5
- [34] Shuzhe Wang, Vincent Leroy, Yohann Cabon, Boris Chidlovskii, and Jerome Revaud. Dust3r: Geometric 3d vision made easy. In *CVPR*, 2024. 6
- [35] Zhou Wang, Alan C Bovik, Hamid R Sheikh, and Eero P Simoncelli. Image quality assessment: from error visibility to structural similarity. *IEEE transactions on image processing*, 13(4):600–612, 2004. 6
- [36] Zhouxia Wang, Ziyang Yuan, Xintao Wang, Yaowei Li, Tianshui Chen, Menghan Xia, Ping Luo, and Ying Shan. Motionctrl: A unified and flexible motion controller for video generation. 2023. 2, 3, 4, 7, 8
- [37] Olivia Wiles, Georgia Gkioxari, Richard Szeliski, and Justin Johnson. SynSin: End-to-end view synthesis from a single image. In *CVPR*, 2020. 1, 2
- [38] Rundi Wu, Ben Mildenhall, Philipp Henzler, Keunhong Park, Ruiqi Gao, Daniel Watson, Pratul P Srinivasan, Dor Verbin, Jonathan T Barron, Ben Poole, et al. Reconfusion: 3d reconstruction with diffusion priors. In *Proceedings of the IEEE/CVF conference on computer vision and pattern recognition*, pages 21551–21561, 2024. 2
- [39] Jianfeng Xiang, Zelong Lv, Sicheng Xu, Yu Deng, Ruicheng Wang, Bowen Zhang, Dong Chen, Xin Tong, and Jiaolong Yang. Structured 3d latents for scalable and versatile 3d generation. *arXiv preprint arXiv:2412.01506*, 2024. 2
- [40] Zeqi Xiao, Yushi Lan, Yifan Zhou, Wenqi Ouyang, Shuai Yang, Yanhong Zeng, and Xingang Pan. Worldmem: Long-term consistent world simulation with memory, 2025. 3
- [41] Jason J Yu, Fereshteh Forghani, Konstantinos G Derpanis, and Marcus A Brubaker. Long-term photometric consistent novel view synthesis with diffusion models. In *Proceedings of the IEEE/CVF International Conference on Computer Vision*, pages 7094–7104, 2023. 2, 3, 4, 6, 7
- [42] Wangbo Yu, Jinbo Xing, Li Yuan, Wenbo Hu, Xiaoyu Li, Zhipeng Huang, Xiangjun Gao, Tien-Tsin Wong, Ying Shan, and Yonghong Tian. Viewcrafter: Taming video diffusion models for high-fidelity novel view synthesis. *arXiv preprint arXiv:2409.02048*, 2024. 1, 2, 7, 8

- [43] Wangbo Yu, Jinbo Xing, Li Yuan, Wenbo Hu, Xiaoyu Li, Zhipeng Huang, Xiangjun Gao, Tien-Tsin Wong, Ying Shan, and Yonghong Tian. ViewCrafter: taming video diffusion models for high-fidelity novel view synthesis. *arXiv*, 2409.02048, 2024. 3
- [44] Shangjin Zhai, Zhichao Ye, Jialin Liu, Weijian Xie, Jiaqi Hu, Zhen Peng, Hua Xue, Danpeng Chen, Xiaomeng Wang, Lei Yang, Nan Wang, Haomin Liu, and Guofeng Zhang. Stargen: A spatiotemporal autoregression framework with video diffusion model for scalable and controllable scene generation, 2025. 3
- [45] Richard Zhang, Phillip Isola, Alexei A Efros, Eli Shechtman, and Oliver Wang. The unreasonable effectiveness of deep features as a perceptual metric. In *Proceedings of the IEEE conference on computer vision and pattern recognition*, pages 586–595, 2018. 6
- [46] Jensen (Jinghao) Zhou, Hang Gao, Vikram Voleti, Aaryaman Vasishtha, Chun-Han Yao, Mark Boss, Philip Torr, Christian Rupprecht, and Varun Jampani. Stable virtual camera: Generative view synthesis with diffusion models. *arXiv preprint arXiv:2503.14489*, 2025. 3, 6, 8
- [47] Tinghui Zhou, Richard Tucker, John Flynn, Graham Fyffe, and Noah Snavely. Stereo magnification: Learning view synthesis using multiplane images. *arXiv preprint arXiv:1805.09817*, 2018. 6, 11

## Appendix

### A. Average Pose Calculation

To compute the average camera pose for rendering surfels, we average translations  $\mathbf{t}_{T+m}$  with a simple mean, and rotations  $\mathbf{R}_{T+m}$  by converting them to quaternions  $\mathbf{q}_m$ , aligning signs to a common hemisphere, and normalizing the mean quaternion:

$$\bar{\mathbf{q}} = \frac{\sum_{m=1}^M \tilde{\mathbf{q}}_m}{\|\sum_{m=1}^M \tilde{\mathbf{q}}_m\|}, \quad \tilde{\mathbf{q}}_m = \text{sign}(\mathbf{q}_m \cdot \mathbf{q}_1) \cdot \mathbf{q}_m.$$

The final average pose is  $\bar{\mathbf{c}} = \begin{bmatrix} \mathbf{R}(\bar{\mathbf{q}}) & \bar{\mathbf{t}} \\ \mathbf{0}^\top & 1 \end{bmatrix}$ , where  $\mathbf{R}(\bar{\mathbf{q}})$  denotes the rotation matrix from  $\bar{\mathbf{q}}$  and  $\bar{\mathbf{t}} = \frac{1}{M} \sum_{m=1}^M \mathbf{t}_{T+m}$ .

### B. Autoregressive Point Map Prediction

Since we generate point maps for each view in an autoregressive manner, it is crucial to maintain their consistency across a shared coordinate space. Point-map estimators such as CUT3R include an optimization stage that jointly refines the depth, camera parameters, and point maps. To ensure a fixed camera trajectory, we freeze the camera parameters, which are user-defined inputs. Additionally, at each generation step when we have  $T$  frames generated so far, we freeze all previously predicted depth maps for frames  $1, 2, \dots, T$  during optimization. This ensures that

the resulting point maps and surfel representations remain consistent and causal. We then save the optimized depth maps of the newly generated frames  $T + 1, \dots, T + M$  for future prediction.

### C. Limitation and Discussion

**Evaluation Protocol.** Since there is no established benchmark for evaluating long-term consistency in scene video generation, we adopt cyclic trajectories as a proxy for assessment. However, these trajectories remain relatively simple and contain only limited occlusions, which means the full potential of VMem in handling occlusions is not fully demonstrated. Moreover, existing evaluation metrics primarily capture low-level texture similarity in hallucinated content, rather than assessing true multi-view consistency—an inherent limitation of single-view perpetual generation. As such, there is a clear need for more standardized evaluation protocols, which we leave for future exploration.

**Limited Training Data and Computing Resources.** Due to limited computational resources, VMem was fine-tuned only on the RealEstate10K dataset [47], which primarily consists of indoor scenes and a limited number of outdoor real-estate scenarios. Consequently, the model may struggle to generalize well to broader contexts. Specifically, performance might degrade when dealing with natural landscapes or images containing moving objects, compared to indoor environments. However, we believe this limitation mainly stems from insufficient dataset diversity and computational constraints.

**Inference Speed.** Due to the multi-step sampling process of diffusion models, VMem requires 4.16 seconds to generate a single frame on an RTX 4090 GPU. This falls short of the real-time performance needed for applications such as virtual reality. We believe that future advancements in single-step image-set models and improvements in computational infrastructure hold promise for significantly accelerating inference speed.

**Future Improvement.** Since our memory module relies heavily on the capabilities of the off-the-shelf image-set model and the point map predictor, the performance of VMem is expected to improve as these underlying models continue to advance.